

Active nematic liquid crystals under a quenched random field

Yutaka Kinoshita and Nariya Uchida*

Department of Physics, Tohoku University, Sendai 980-8578, Japan

(Dated: June 4, 2025)

Coupling between flow and orientation is a central issue in understanding the collective dynamics of active biofilaments and cells. Active stresses generated by motor activity destroy (quasi-)long-range orientational order and induce chaotic flows with many vortices. In cellular and subcellular environment, alignment is also hindered by heterogeneous filamentous structures in extracellular matrix and various intracellular organelles. Here we address the effects of a quenched random field on the flow patterns and orientational order in two-dimensional active nematic liquid crystals. We find that the director dynamics becomes frozen above a critical disorder strength. For sufficiently strong randomness, the orientational correlation function decays exponentially with distance, reproducing the behavior of passive random-field nematics. In contrast, the flow velocity decreases only gradually with increasing disorder, and exhibits a logarithmic spatial correlation under strong randomness. We identify the threshold between the activity- and disorder-dominated regimes and examine its dependence on the activity parameter.

Introduction. – Collective motion of cells and biofilaments is of vital importance to life at various stages, such as cell division, morphogenesis, cell migration, and apoptosis. The dynamics are driven by molecular motors and facilitated by orientational ordering of active elements with slender shapes. While apolar interaction induces nematic order, active stresses generated by motor activity destroy (quasi-)long-range orientational order and generate chaotic flows with many vortices, which are known as active turbulence [1–3]. Active nematic turbulence has been demonstrated in a two-dimensional suspension of microtubules and kinesin-motor-complexes [4]. Topological defects are also found in colonies of cells [5–7] and multicellular organisms [8], and their biological functions have been revealed.

The flow patterns of active nematics can be controlled by friction with the substrate [9–14], external fields [15–17], and confinement [18–23]. Theoretical studies have examined the effects of uniform external fields, such as in a model of an active pump using a Frederiks twisted cell [15]. A three-dimensional simulation of active nematics under an electric field found a direct transition from active turbulence to a uniformly aligned state [16], while a laning state intervenes in two dimensions [17]. Laning states are also obtained in numerical simulations with isotropic [12, 13] or anisotropic [14] friction, and have also been explored experimentally [9]. Confinement also results in various director patterns such as the laning state and vortex lattice [19–23]. Recently, attention has shifted toward couplings of active nematics with non-uniform fields, such as friction from micropatterned surfaces [24], curvature of epithelial tissues [25], spatially varying activity [26, 27], and composition [28].

On the other hand, the behavior of active nematics in a randomly heterogeneous environment is an open issue. Cells in tissues are in contact with the extracellular matrix which contains fibrous material such as collagen and cellulose. Collagen fibers form anisotropic networks that guide the migration of cells [29]. Plant cellulose is also used as a scaffold for in vitro

culture of neural stem cells [30]. Microtubules in cells are entangled with other components of the cytoskeletal network such as actins and intermediate filaments, which hinder alignment. The cytoplasm also contains a number of proteins that cyclically change their shapes and generate random hydrodynamic forces. They not only enhance diffusion in the cell [31], but may also contribute to the disorientation of active cytoskeletal filaments. To elucidate the effects of heterogeneous anisotropic environments on active nematic flows, we address the effects of quenched random fields in this paper.

The effect of a quenched random field on nematic liquid crystals has been studied in a model of nematic elastomers [32]. The numerical study showed that the orientational correlation function decays exponentially as a function of distance, and that the correlation length also decays exponentially with the disorder strength.

Recently, the effects of a random field on dry and wet active nematics have been addressed in Refs. [33, 34]. In both cases, the quenched disorder slows the dynamics of topological defects. The orientational correlation function exhibits a crossover from algebraic to exponential decay for dry active nematics, whereas wet active nematics display a slow coarsening behavior. However, the flow behavior of active nematics under quenched randomness remains largely unexplored, despite its potential importance in cytoskeletal dynamics and the collective migration of cell colonies.

In the present paper, we focus on the flow behavior and show that its response to quenched randomness is in marked contrast with that of the orientational order. We also vary the randomness over a wide range and identify a transition from the weak to strong disorder regimes for wet active nematics.

Model. – The orientational order of a two-dimensional nematic liquid crystal is described by the symmetric and traceless tensor $Q_{ij} = S \left(n_i n_j - \frac{1}{2} \delta_{ij} \right)$, where S is the scalar order parameter and $\mathbf{n} = (\cos \theta, \sin \theta)$ is the director. The dynamical equations of active nematics in the dimensionless form read [2]

$$(\partial_t + \mathbf{v} \cdot \nabla) \mathbf{v} = \frac{1}{\text{Re}} \nabla^2 \mathbf{v} - \nabla p + \nabla \cdot \boldsymbol{\sigma} \quad (1)$$

* nariya.uchida@tohoku.ac.jp

and

$$(\partial_t + \mathbf{v} \cdot \nabla) \mathbf{Q} = \lambda S \mathbf{u} + \mathbf{Q} \cdot \boldsymbol{\omega} - \boldsymbol{\omega} \cdot \mathbf{Q} + \gamma^{-1} \mathbf{H}. \quad (2)$$

Here, \mathbf{v} is the normalized flow velocity, which satisfies the incompressibility condition $\nabla \cdot \mathbf{v} = 0$, p is the pressure and $\boldsymbol{\sigma}$ is the stress tensor. The flow properties are characterized by the Reynolds number Re , the flow alignment parameter λ , and the rotational viscosity γ , and $u_{ij} = (\partial_i v_j + \partial_j v_i)/2$ and $\omega_{ij} = (\partial_i v_j - \partial_j v_i)/2$ are the symmetric and antisymmetric parts of velocity gradient tensor, respectively. We hereafter refer to $\boldsymbol{\omega} = \omega_{xy}$ as the vorticity. We assume $0 < \lambda < 1$; a positive value of λ corresponds to elongated or rod-like elements and $|\lambda| < 1$ places the system in the flow-tumbling regime, where no stable director orientation exists in a uniform shear flow [35, 36]. The molecular field H_{ij} is the symmetric and traceless part of $-\delta F/\delta Q_{ij}$, and is obtained from the Landau-de Gennes free energy [35]

$$F = \int f d^2 r, \quad (3)$$

$$f = \frac{A}{2} \text{Tr} \mathbf{Q}^2 + \frac{C}{4} (\text{Tr} \mathbf{Q}^2)^2 + \frac{K}{2} (\nabla \mathbf{Q})^2 - \frac{1}{2} \mathbf{E} \cdot \mathbf{Q} \cdot \mathbf{E}. \quad (4)$$

The first two terms of the free energy density control the magnitude of the scalar order parameter S . Note that the term proportional to $\text{Tr} \mathbf{Q}^3$ identically vanishes for the two-dimensional nematic order parameter. The third term is the Frank elastic energy under the one-constant approximation, and the fourth term describes the coupling to the quenched random field \mathbf{E} . The molecular field is obtained as

$$H_{xx} = -\left(2A + CS^2\right) Q_{xx} + 2K \nabla^2 Q_{xx} + \frac{1}{2} (E_x^2 - E_y^2). \quad (5)$$

$$H_{xy} = -\left(2A + CS^2\right) Q_{xy} + 2K \nabla^2 Q_{xy} + E_x E_y. \quad (6)$$

The stress tensor consists of the passive stress

$$\boldsymbol{\sigma}^e = -\lambda S \mathbf{H} + \mathbf{Q} \cdot \mathbf{H} - \mathbf{H} \cdot \mathbf{Q}, \quad (7)$$

and the active stress

$$\boldsymbol{\sigma}^a = -\alpha \mathbf{Q}. \quad (8)$$

We assume an extensile active stress, so the activity parameter α is positive.

We model the quenched random field as

$$\mathbf{E} = E_0 \mathbf{e}(\mathbf{r}) \quad (9)$$

where $\mathbf{e}(\mathbf{r}) = (\cos \theta_e, \sin \theta_e)$ is a random unit vector where the angle θ_e is uniformly distributed in $[0, 2\pi)$. In most of our numerical simulations, we implement the random field on a square lattice with the grid size Δx , and choose the angle θ_e randomly at each grid point. Therefore, it satisfies

$$\langle \mathbf{e}(\mathbf{r}) \mathbf{e}(\mathbf{r}') \rangle = \frac{1}{2} \mathbf{I} \delta_{\mathbf{r}, \mathbf{r}'}, \quad (10)$$

where $\delta_{\mathbf{r}, \mathbf{r}'}$ is the Kronecker delta defined on a lattice. In the continuum limit, where the typical length scale is much larger than Δx , it is convenient to replace it with the expression

$$\langle \mathbf{e}(\mathbf{r}) \mathbf{e}(\mathbf{r}') \rangle = \frac{(\Delta x)^2}{2} \mathbf{I} \delta(\mathbf{r} - \mathbf{r}'). \quad (11)$$

The contributions of the random field and Frank elasticity to the free energy are estimated as $E_0^2 S_0$ and $K S_0^2 / l_Q^2$, respectively, where S_0 is the typical magnitude of the scalar order parameter and l_Q is the correlation length of \mathbf{Q} . The orientational correlation length decreases with increasing disorder strength, and its lower bound is given by $l_Q \sim \Delta x$. Therefore, we define the effective disorder strength as

$$D_K = \frac{E_0^2 (\Delta x)^2}{K S_0}. \quad (12)$$

On the other hand, the contributions to the molecular field by the random field and the active stress are estimated as E_0^2 and α , respectively. Thus we are led to the other definition of the dimensionless disorder strength,

$$D_\alpha = \frac{E_0^2}{\alpha}. \quad (13)$$

Disorder-dominated regime. – In the disorder-dominated regime with $D_K \gg 1$ and $D_\alpha \gg 1$, the director aligns with the local random field and becomes frozen. In this case, we have approximately $\mathbf{n}(\mathbf{r}) = \mathbf{e}(\mathbf{r})$, $\mathbf{H} = \mathbf{0}$ and $\boldsymbol{\sigma}^e = \mathbf{0}$ in the stationary state, and the Frank elastic term in the molecular field is negligible. Thus, from Eqs.(5),(6), the scalar order parameter satisfies

$$-S \left(2A + CS^2\right) + E_0^2 = 0, \quad (14)$$

whose solution defines S_0 . The nematic order parameter is given by

$$\mathbf{Q}(\mathbf{r}, t) = S_0 \left[\mathbf{e}(\mathbf{r}) \mathbf{e}(\mathbf{r}) - \frac{1}{2} \mathbf{I} \right]. \quad (15)$$

Since the molecular field vanishes in the steady state, the flow velocity is determined solely by the active stress. For $\text{Re} \ll 1$, the velocity field is obtained by neglecting the terms on the left hand side of Eq.(1) as

$$0 = \frac{1}{\text{Re}} \nabla^2 \mathbf{v} - \nabla p + \nabla \cdot \boldsymbol{\sigma}^a. \quad (16)$$

Solving (16) under the incompressibility condition and with (8), we obtain the velocity field in the Fourier representation,

$$\mathbf{v}^k = -\alpha \text{Re} \frac{\mathbf{I} - \hat{k} \hat{k}}{k^2} \cdot (i \mathbf{k} \cdot \mathbf{Q}^k), \quad (17)$$

which yields the velocity structure factor

$$\begin{aligned} \Sigma_v(\mathbf{k}) &= \langle |\mathbf{v}^k|^2 \rangle \\ &= \frac{(\alpha \text{Re})^2}{k^2} \left(\langle |\hat{k} \cdot \mathbf{Q}^k|^2 \rangle - \langle \hat{k} \cdot \mathbf{Q}^k \cdot \hat{k} \rangle \right). \end{aligned} \quad (18)$$

The correlation function of the nematic order parameter is obtained from from Eqs.(11,15) as

$$\langle Q_{ij}(\mathbf{r})Q_{lm}(\mathbf{r}') \rangle = \frac{1}{4}S_0^2(\Delta x)^2 (\delta_{il}\delta_{jm} + \delta_{im}\delta_{jl}) \delta(\mathbf{r} - \mathbf{r}'), \quad (19)$$

and accordingly

$$\langle Q_{ij}^k Q_{lm}^{-k} \rangle = \frac{1}{4}S_0^2(\Delta x)^2 (\delta_{il}\delta_{jm} + \delta_{im}\delta_{jl}). \quad (20)$$

Substituting this into Eq.(18), we obtain

$$\Sigma_v(\mathbf{k}) = \frac{(\alpha \text{Re} S_0 \Delta x)^2}{4k^2}. \quad (21)$$

The velocity correlation function in the real space is given by the inverse Fourier transform of $\Sigma_v(\mathbf{k})$ as

$$\langle \mathbf{v}(\mathbf{r}) \cdot \mathbf{v}(\mathbf{r}') \rangle = -\frac{(\alpha \text{Re} S_0 \Delta x)^2}{8\pi} \ln |\mathbf{r} - \mathbf{r}'|. \quad (22)$$

Numerical simulation. – We solved Eqs. (1,2) numerically on a square lattice with the fourth-order Runge-Kutta method. We enforced the incompressibility condition using the simplified MAC method on a staggered lattice [37]. The main sublattice is used for the field variables \mathbf{Q} , p , $\boldsymbol{\sigma}$, \mathbf{u} , $\boldsymbol{\omega}$ and \mathbf{H} , and the other two sublattices are assigned to v_x and v_y . The calculation is performed on a $N_x \times N_y$ lattice with the grid size $\Delta x = \Delta y = 2$ and the step time increment $\Delta t = 0.01$. We imposed periodic boundary conditions and used the Fast Fourier Transform to solve the Poisson equation for the pressure at each time step. For the numerical analysis, we used the parameter values

$$A = -0.16, C = 0.89, K = 1, \quad (23)$$

$$\lambda = 0.1, \text{Re} = 0.1, \gamma = 10. \quad (24)$$

We varied the activity parameter α from -0.2 to 0.2 to study both extensile and contractile systems. In most of our simulations, the direction $\mathbf{e}(\mathbf{r})$ of the random field was randomly chosen at each grid point. The field strength is varied in the range $0 \leq E_0 \leq 0.7$. We have also checked the effects of a spatially correlated random field, which is prepared by solving the diffusion equation for \mathbf{E} starting from the grid-wise random field and normalizing the amplitude to E_0 . The resulting random field has an approximately Gaussian correlation function $C_E(\mathbf{r} - \mathbf{r}') = \langle \mathbf{E}(\mathbf{r}) \cdot \mathbf{E}(\mathbf{r}') \rangle$. We define the standard deviation of this distribution as the disorder correlation length ξ_E . We studied the cases $\xi_E = 4.0, 6.0, 8.0$, in addition to the grid-wise random field, which gives $\xi_E = 2(1 - e^{-1/2}) \approx 0.8$. The scalar order parameter in the passive ($\alpha = 0$) and stationary system is obtained from Eq. (14) as $S_0 \approx 0.60$ for $E_0 = 0$ and increases with E_0 . We confirmed that S does not exceed unity for the strongest random field studied ($E_0 = 0.7$). The defect core radius is given by $\xi = \sqrt{K/|A|} \approx 2.5$. The balance between the activity and Frank elasticity defines the length scale $l_\alpha = \sqrt{K/|\alpha|}$, which gives $l_\alpha \approx 2.2$ for $|\alpha| = 0.2$ and $l_\alpha \approx 3.2$ for $|\alpha| = 0.1$. Thus we have ensured that l_α exceeds

the grid size. The system size is fixed to $N_x = N_y = 256$ so that $L = N_x \Delta x = N_y \Delta y = 512$. For the initial conditions, we initialized the velocity to zero and imposed small random fluctuations around zero for $\mathbf{Q}(\mathbf{r}, 0)$, assuming a quench from the isotropic quiescent state. Specifically, the scalar order parameter and the director angle at each grid point are randomly chosen in the intervals $[0, 0.1]$ and $[0, 2\pi]$, respectively. We observed the total kinetic energy as a function of time to confirm that the system reached a dynamical steady state, typically by $t = 10000$ in active turbulence regimes. We calculated the data over the time window $20000 < t \leq 40000$ with the time interval $t_0 = 100$, and took the ensemble average over 8 independent realizations.

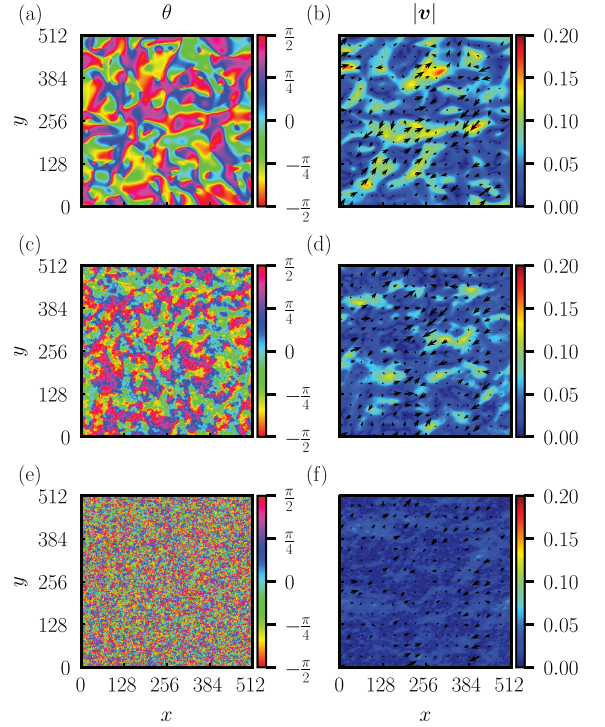


FIG. 1. Snapshots of the director angle $\theta(x, y)$ (first column) and the velocity field $\mathbf{v}(x, y)$ (second column), where the color indicates the magnitude and black arrows represent the vector field. The activity is fixed at $\alpha = 0.2$, and the random field strengths are (a)(b) $E_0 = 0$, (c)(d) $E_0 = 0.4$, and (e)(f) $E_0 = 0.7$.

Spatial patterns and orientational freezing. – In Fig. 1, we show the snapshots of the director angle $\theta(\mathbf{r}, t)$ and the vorticity $\omega(\mathbf{r}, t)$ in the dynamical steady states for $\alpha = 0.2$. For $E_0 = 0$, active turbulence containing topological defects and vortices is reproduced [Fig.1(a)(b)]. For $E_0 = 0.4$, the director pattern becomes jagged while maintaining the characteristic large-scale structure of nematic defects. The velocity field is smoother but streamlines with wavy shapes appear [Fig.1(c)(d)]. For $E = 0.7$, the director orientation becomes completely random, and the flow pattern obtains streak-like structures of various sizes [Fig.1(e)(f)].

The dynamics slow down as we increase the field strength. In Fig. 2, we show the mean square of the time derivative of the order parameter \dot{Q}_{ij} and flow velocity. The time

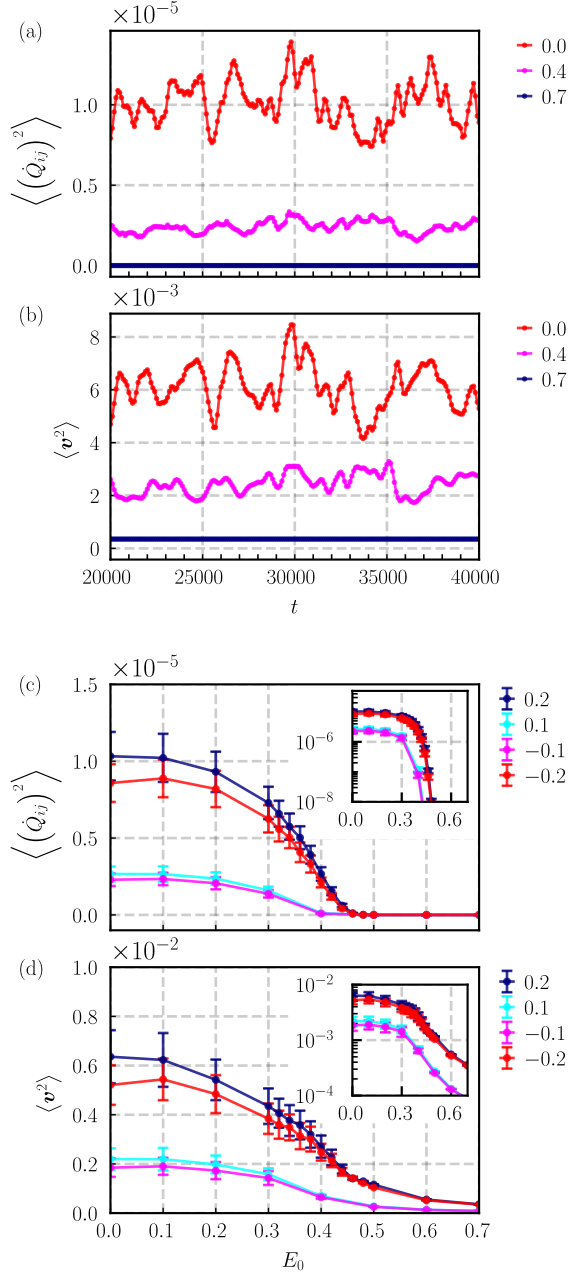


FIG. 2. Mean square of the time derivative of Q_{ij} and the flow velocity v for $\alpha = 0.2$. (a), (b): Time evolution for a single sample, at $E_0 = 0.0, 0.4, 0.7$. (c), (d): Averages over time and 8 samples, plotted as functions of the random field strength E_0 for $\alpha = 0.2, 0.1, -0.1, -0.2$. Error bars represent the standard deviation. Insets: semi-logarithmic plots.

evolution of these quantities for $20000 < t \leq 40000$ is shown in Fig. 2(a),(b), for $\alpha = 0.2$ fixed and $E_0 = 0, 0.4$ and 0.7 . These quantities exhibit large fluctuations around their mean values, with a typical timescale $\sim 10^3$ for $E_0 = 0.0$. Both the mean values and fluctuations get smaller as E_0 is increased. For $E_0 = 0.7$, $\langle \dot{Q}_{ij}^2 \rangle$ vanishes, while the velocity maintains a small but finite magnitude. These data justify using statistical

averages over the same time window to be shown in the rest of this paper. In Fig. 2(c),(d), we show the time-averaged values for $\alpha = 0.2, 0.1, -0.1$ and -0.2 as functions of E_0 . We find that the extensile ($\alpha > 0$) and contractile ($\alpha < 0$) cases show qualitatively similar behavior. Quantitatively, the extensile systems exhibit values approximately 10 – 20% larger than the contractile cases with the same magnitude of $|\alpha|$, for both \dot{Q}_{ij}^2 and v^2 and for $E_0 \leq 0.4$. For $E_0 \geq 0.5$, the differences between them become very small. The ratios of these quantities between $\alpha = 0.2$ and $\alpha = 0.1$ are about 4 for \dot{Q}_{ij}^2 and 3 for v^2 at $E_0 = 0$. For $\alpha = 0.2$, \dot{Q}_{ij}^2 shows a sharp drop below 10^{-6} at $E_0 = 0.44$, while a similar drop occurs at a smaller E_0 for $\alpha = 0.1$; see the semi-log plots in the inset of Fig. 2(c). We henceforth focus on the extensile case $\alpha = 0.2$. The director dynamics completely freeze at $E_0 \approx 0.5$. On the other hand, the mean square velocity decreases only gradually as we increase the disorder strength. Its decay for $E_0 > 0.44$ is slower than that of the orientational order parameter. For $E_0 = 0.7$, the strongest field we studied, the mean square velocity still remains at approximately 6 % of its value at $E_0 = 0$. Note that the effective disorder strengths are $D_K \simeq 0.97$ and $D_\alpha \simeq 0.96$ for $E_0 = 0.44$, which are both close to unity. Therefore, it would be reasonable to distinguish the medium and strong disorder regimes at this value of E_0 . We also examined the dynamics under a spatially correlated random field. As we increase ξ_E from 0.8 to 8.0 with the fixed amplitude $E_0 = 0.4$, $\langle \dot{Q}_{ij}^2 \rangle$ decreases from 2.6×10^{-6} to 7.0×10^{-12} , indicating that the director dynamics depends significantly on the random-field correlation length. On the other hand, $\langle v^2 \rangle$ shows only minor decrease from 2.7×10^{-3} to 1.9×10^{-3} . Thus, the remnant flow in the orientationally frozen state is robust and only weakly dependent on the structure of the random field.

Correlation functions and correlation lengths. – In Fig. 3, we show the spatial correlation functions for the orientational order parameter and flow velocity, which are defined by

$$C_Q(r) = \frac{\langle Q(\mathbf{r} + \mathbf{r}', t) : Q(\mathbf{r}', t) \rangle}{\langle Q(\mathbf{r}', t)^2 \rangle} \quad (25)$$

and

$$C_v(r) = \frac{\langle v(\mathbf{r} + \mathbf{r}', t) \cdot v(\mathbf{r}', t) \rangle}{\langle v(\mathbf{r}', t)^2 \rangle}, \quad (26)$$

respectively, where $\langle \dots \rangle$ denotes averages over \mathbf{r}' and t , and 8 independent realizations. By symmetry, the correlation functions depend only on the distance r . We show their profiles along the x -axis in Fig. 3. We again confirm that the extensile case ($\alpha = 0.2$) and contractile case ($\alpha = -0.2$) show similar behaviors for $E_0 = 0.0$, we henceforth focus on the extensile case in the following, and vary the field strength as $E_0 = 0.0, 0.4$, and 0.7 . The orientational correlation function $C_Q(r)$ decreases monotonically with positive curvature [Fig. 3(a)]. For $E_0 = 0.7$, it is well fitted by the exponential function $C_Q(r) = \exp(-r/r_Q)$ with $r_Q = 2.3$. The fitting range is $2 \leq r \leq 10$. The semi-logarithmic plot in the inset of Fig. 3(a) shows that the exponential decay also holds for the medium

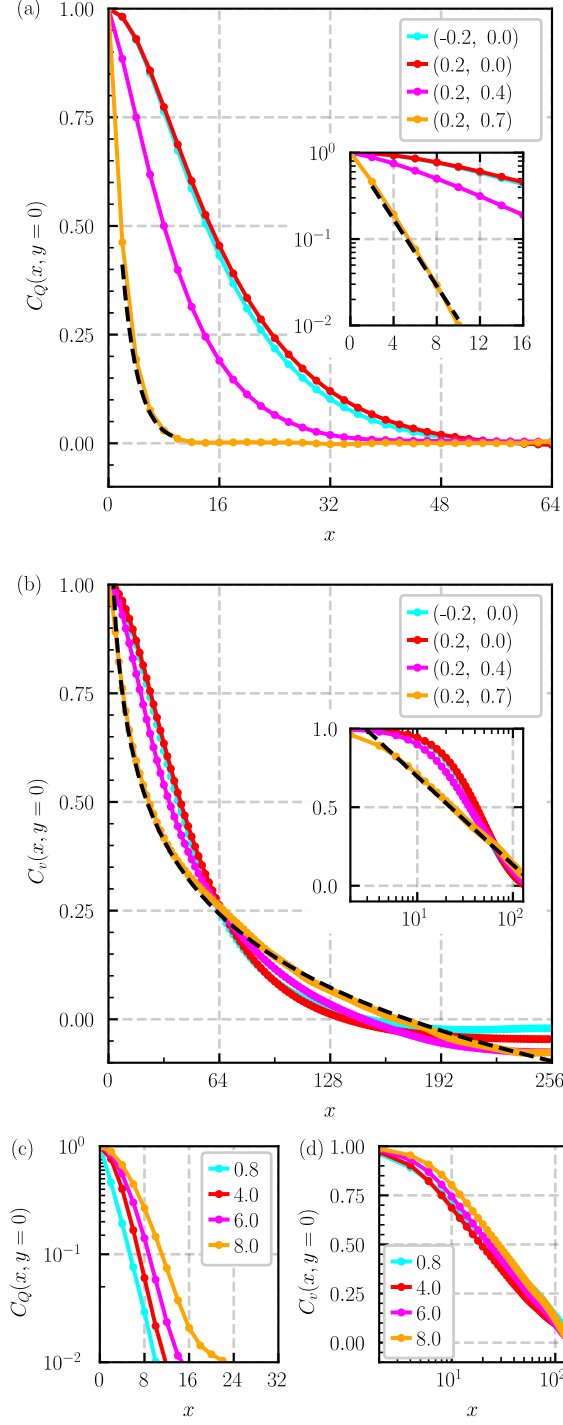


FIG. 3. Orientational and velocity correlation functions. (a), (b): $(\alpha, E_0) = (-0.2, 0.0), (0.2, 0.0), (0.2, 0.4), (0.2, 0.7)$ with $\xi_E = 0.8$. (c), (d): $(\alpha, E_0) = (0.2, 0.7)$ with $\xi_E = 0.8, 2.0, 4.0, 8.0$. (a): $C_Q(r)$ (inset: semilog-y plot). Dashed lines indicate the fitting function $\exp(-r/r_Q)$ with $r_Q = 2.3$. (b): $C_v(r)$ (inset: semilog-x plot). Dashed line indicates the fitting function $-A \ln(r/r_v)$ with $A = 0.25$ and $r_v = 173$. (c): $C_Q(r)$ (semilog-y plot). (d): $C_v(r)$ (semilog-x plot).

disorder case $E_0 = 0.4$, up to $r \approx 30$, while the decay is faster than exponential for $E_0 = 0$ as seen from the upward-convex shape in the semi-log plot. Furthermore, for $E_0 = 0.7$, we confirmed that the orientational correlation functions for $-0.2 \leq \alpha \leq 0.2$ closely match each other; the data are not shown as they are indistinguishable at the scale of Fig. 3(a).

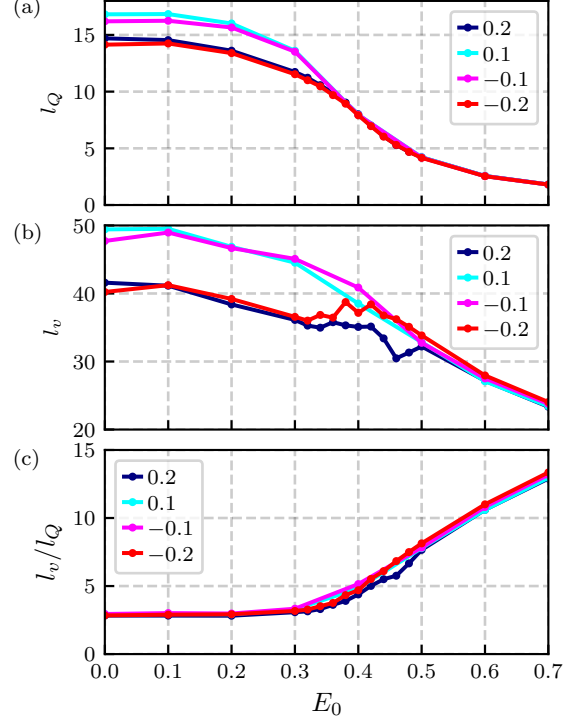


FIG. 4. (a) Orientational correlation length l_Q , (b) velocity correlation length l_v , and (c) the ratio l_v/l_Q as functions of the random field strength E_0 .

The velocity correlation function decays more slowly than the orientational one, and turns negative at $r \sim L/4$ for $E_0 = 0$ and at $r \sim L/3$ for $E_0 = 0.7$ [Fig. 3(b)]. It decreases monotonically up to $r = 0.5L$ and is expected to converge to zero for $r \rightarrow \infty$. The function has a negative curvature in a narrow range near $r = 0$, which becomes narrower for a larger field strength. For $E_0 = 0.7$, it is well fitted by the logarithmic function $C_v(r) = -A \ln(r/r_v)$ over the range $2 \leq r < L/2$, yielding $A = 0.24$ and $r_v = 173$. In addition, for a $L = 256$ system, we found that the same fitting gives $r_v = 78$, suggesting that r_v is determined by, and proportional to, the system size.

To investigate the effects of a spatially correlated random field, we show the orientational and velocity correlation functions for $\xi_E = 0.8, 4.0, 6.0, 8.0$ in Fig. 3(c)(d), where $\alpha = 0.2$ and $E_0 = 0.7$ are fixed. We find that $C_Q(r)$ decays approximately exponentially for $r > \xi_E$, while it shows a slower decay for $r < \xi_E$ and at large distances where $C_Q(r) \ll 0.1$. On the other hand, $C_v(r)$ in the semilog-x plot shows a constant slope over a wide range ($8 < r < 50$) for all cases, while the decay is slower near the origin. These results confirm the robustness

of the exponential and logarithmic decay of $C_Q(r)$ and $C_v(r)$, respectively.

We define the correlation lengths l_Q and l_v by $C_Q(l_Q) = 1/2$ and $C_v(l_v) = 1/2$, respectively. They are plotted in Fig. 4(a)(b) as functions of the field strength. The orientational correlation length shows a rapid decay between $E_0 = 0.2$ and 0.5 . The decay of the velocity correlation length is slower, and exhibits large fluctuations in the transition region $0.3 < E_0 < 0.5$, reflecting sample dependence. The ratio l_v/l_Q , as shown in Fig. 4(c), increases to 13 at $E_0 = 0.7$ from 2.8 at $E_0 = 0$.

Discussion. – We found a marked contrast between the orientational and flow properties, which can be summarized as follows: (i) The dynamics of the orientational order parameter freezes completely at and above a critical random field strength, while the flow velocity only gradually decreases with increased randomness and remains finite even in the strong disorder limit. (ii) The spatial correlation of the orientational order parameter is short-ranged and exhibits exponential decay for strong disorder, while the flow velocity retains long-range correlations, characterized by logarithmic decay for strong disorder. We have also compared the extensile and contractile systems, and found only minor differences between the two when the magnitude of activity $|\alpha|$ is the same. The difference becomes negligible in the strong disorder regime.

The exponential decay of the orientational correlation function $C_Q(r)$ in the strong disorder regime [Fig. 3(a)] agrees with the previous result on 2D random-field nematics [32]. This suggests that the director texture is determined by the balance between the random field and Frank elasticity, and is only weakly affected by the active flow. This is supported by the fact that $C_Q(r)$ for $-0.2 \leq \alpha \leq 0.2$ are nearly indistinguishable from each other for $E_0 = 0.7$. Earlier studies on the random-field XY model reported correlation decaying faster than exponential in two dimensions [38, 39]. The difference is attributed to the difference in the symmetry of the random anisotropy in nematics and the XY model [32]. Without the randomness, the orientational correlation function decays faster than exponentially as seen in Fig. 3(a). In this case, the correlation functions are characterized by the vortex size [40], and the velocity correlation function $C_v(r)$ has a negative curvature at short distances, as seen in Fig. 3(b), which agrees with the analytical result [40]. As we increase the random field, the range with a negative curvature shrinks and the velocity correlation function is better approximated by the logarithmic function. This is in agreement with the analytical result for the strong disorder [Eq.(22)], and reflects the structure of the Green function of the Stokes equation in two dimensions. In three dimensions, the velocity correlation function should decay as $1/r$ in the strong disorder limit. Note that we cannot fully reach the strong disorder limit in our numerical simulations. The effective disorder strengths are $D_K \simeq 2.0$ and $D_\alpha \simeq 2.5$ for $E_0 = 0.7$ and $\alpha = 0.2$. In addition, the orientational correlation length $r_Q = 2.3$ for $E_0 = 0.7$ is close to the grid size Δx . The amplitude E_0 was not increased further in order to ensure that the scalar order parameter remained within a physically reasonable range and that the correlation length stayed larger than the grid size.

Still, the logarithmic function for the velocity correlation fits the numerical results well, with errors within $\pm 6\%$ over the range $4 \leq r \leq 110$, where $C_v(r) \geq 0.1$. The error increases to 16% at $r = \Delta x = 2$ due to the discreteness of the lattice. These findings confirm the validity of the analytical results obtained by the continuum approximation over a wide distance range.

The dependence of the orientational and velocity correlation lengths on the field strength is also in marked contrast. For weak disorder, both lengths are proportional to the vortex size and the ratio l_v/l_Q is small. For strong disorder, the velocity correlation decays monotonically even when the orientational correlation length approaches a constant, and thus l_v/l_Q diverges in the strong disorder limit. The slowing down of the increase of l_v/l_Q in the strong disorder regime [Fig. 4(b)] is explained by the fact that l_Q has a lower bound determined by the defect core size, and that l_v has an upper bound determined by the system size. (Note that l_v cannot exceed $L/2$ due to the periodic boundary condition.) Since the Stokes equation lacks a characteristic length scale, it is natural that l_v is proportional to the system size.

Finally, we consider the competition between the active flow and the random field. The flow-aligning effect on the nematic order parameter is represented by the term $\lambda S \mathbf{u}$ in Eq. (2), the magnitude of which is estimated as $\lambda S_0 v_{\text{rms}}/l_v$. The contribution of the random field to the term $\gamma^{-1} \mathbf{H}$ is estimated as $\gamma^{-1} E_0^2 S_0$. Averaging it over the area l_Q^2 of an orientationally correlated region, which contains $N \sim (l_Q/\Delta x)^2$ sites, we get $\gamma^{-1} E_0^2 S_0/\sqrt{N} \sim \gamma^{-1} E_0^2 S_0 \Delta x/l_Q$. Thus the ratio between the flow-aligning and random-field terms is estimated as $\gamma \lambda v_{\text{rms}} l_Q/(E_0^2 l_v \Delta x)$. In our simulation, this ratio becomes 0.33 for $E_0 = 0.2$ and $\alpha = 0.2$, which supports the observation that the active flow has a minor effect in the medium ($0.2 < E_0 < 0.44$) and strong ($E_0 > 0.44$) disorder regimes. It is also consistent with the fact that the mean flow velocity and correlation lengths start to decrease around $E_0 = 0.2$. Note that the dependence of this ratio on the activity parameter and the random field strength arises mainly from the v_{rms} and $1/E_0^2$ and that the former is proportional to α in the weak disorder regime. The other factor l_Q/l_v also depends on α and E_0 but more weakly: $l_Q \sim l_\alpha \propto |\alpha|^{-1/2}$ in the weak disorder regime, and l_Q/l_v changes roughly linearly with E_0 in the strong disorder regime [Fig. 4(c)]. Therefore, the main differences in the system's behavior due to the activity and disorder strength can be attributed to the active stress ($\propto \alpha$) and the random field free energy ($\propto E_0^2$), which enter the dynamical equations.

In summary, quenched disorder introduces distinctive effects into the physics of active nematics. In the strong disorder regime, the director texture becomes frozen and is governed by the balance between the randomness and Frank elasticity, while the active flow persists with long-range correlations and facilitates material transport. We hope that the present work will stimulate experimental studies on the flow properties of cellular and subcellular systems with orientational order.

Acknowledgements. – Y.K. acknowledges support of the work through the International Joint Graduate Program in Materials Science at Tohoku University and JST SPRING, Grant

-
- [1] H. H. Wensink, J. Dunkel, S. Heidenreich, K. Drescher, R. E. Goldstein, H. Löwen, and J. M. Yeomans, *Proc. Natl. Acad. Sci. U.S.A.* **109**, 14308 (2012).
 - [2] A. Doostmohammadi, J. Ignés-Mullol, J. M. Yeomans, and F. Sagués, *Nat. Commun.* **9**, 1 (2018).
 - [3] R. Alert, J. Casademunt, and J.-F. Joanny, *Ann. Rev. Condens. Matter Phys.* **13**, 143 (2022).
 - [4] T. Sanchez, D. T. Chen, S. J. DeCamp, M. Heymann, and Z. Dogic, *Nature* **491**, 431 (2012).
 - [5] A. Doostmohammadi, S. P. Thampi, and J. M. Yeomans, *Phys. Rev. Lett.* **117**, 048102 (2016).
 - [6] T. B. Saw, A. Doostmohammadi, V. Nier, L. Kocgozlu, S. Thampi, Y. Toyama, P. Marcq, C. T. Lim, J. M. Yeomans, and B. Ladoux, *Nature* **544**, 212 (2017).
 - [7] K. Kawaguchi, R. Kageyama, and M. Sano, *Nature* **545**, 327 (2017).
 - [8] Y. Maroudas-Sacks, L. Garion, L. Shani-Zerbib, A. Livshits, E. Braun, and K. Keren, *Nat. Phys.* **17**, 251 (2021).
 - [9] P. Guillamat, J. Ignés-Mullol, and F. Sagués, *Proc. Natl. Acad. Sci. U.S.A.* **113**, 5498 (2016).
 - [10] P. Guillamat, J. Ignés-Mullol, S. Shankar, M. C. Marchetti, and F. Sagués, *Phys. Rev. E* **94**, 060602(R) (2016).
 - [11] P. Guillamat, J. Ignés-Mullol, and F. Sagués, *Nat. Commun.* **8**, 1 (2017).
 - [12] S. P. Thampi, R. Golestanian, and J. M. Yeomans, *Phys. Rev. E* **90**, 062307 (2014).
 - [13] P. Srivastava, P. Mishra, and M. C. Marchetti, *Soft Matter* **12**, 8214 (2016).
 - [14] K. Thijssen, L. Metselaar, J. M. Yeomans, and A. Doostmohammadi, *Soft Matter* **16**, 2065 (2020).
 - [15] R. Green, J. Toner, and V. Vitelli, *Phys. Rev. Fluids* **2**, 104201 (2017).
 - [16] Ž. Krajnik, Ž. Kos, and M. Ravnik, *Soft Matter* **16**, 9059 (2020).
 - [17] Y. Kinoshita and N. Uchida, *Phys. Rev. E* **108**, 014605 (2023).
 - [18] L. Giomi, L. Mahadevan, B. Chakraborty, and M. Hagan, *Nonlinearity* **25**, 2245 (2012).
 - [19] A. Doostmohammadi, T. N. Shendruk, K. Thijssen, and J. M. Yeomans, *Nat. Commun.* **8**, 1 (2017).
 - [20] T. N. Shendruk, A. Doostmohammadi, K. Thijssen, and J. M. Yeomans, *Soft Matter* **13**, 3853 (2017).
 - [21] M. M. Norton, A. Baskaran, A. Opatthalage, B. Langeslay, S. Fraden, A. Baskaran, and M. F. Hagan, *Phys. Rev. E* **97**, 012702 (2018).
 - [22] R. C. Coelho, N. A. Araújo, and M. M. T. da Gama, *Soft Matter* **15**, 6819 (2019).
 - [23] C. Rorai, F. Toschi, and I. Pagonabarraga, *Phys. Rev. Fluids* **6**, 113302 (2021).
 - [24] K. Thijssen, D. A. Khaladj, S. A. Aghvami, M. A. Gharbi, S. Fraden, J. M. Yeomans, L. S. Hirst, and T. N. Shendruk, *Proc. Natl. Acad. Sci. U.S.A.* **118**, e2106038118 (2021).
 - [25] F. Vafa and L. Mahadevan, *Phys. Rev. Lett.* **129**, 098102 (2022).
 - [26] J. Rønning, M. C. Marchetti, and L. Angheluta, *R. Soc. Open Sci.* **10**, 221229 (2023).
 - [27] A. Partovifard, J. Grawitter, and H. Stark, *Soft Matter* **20**, 1800 (2024).
 - [28] R. Assante, D. Corbett, D. Marenduzzo, and A. Morozov, *Soft Matter* **19**, 189 (2023).
 - [29] G. Thrivikraman, A. Jagiełło, V. K. Lai, S. L. Johnson, M. Keating, A. Nelson, B. Schultz, C. M. Wang, A. J. Levine, E. L. Botvinick, and R. T. Tranquillo, *Proc. Natl. Acad. Sci. U.S.A.* **118**, e2024942118 (2021).
 - [30] L. J. Couvrette, K. L. Walker, T. V. Bui, and A. E. Pelling, *Bioengineering* **10**, 1309 (2023).
 - [31] A. S. Mikhailov and R. Kapral, *Proc. Natl. Acad. Sci. U.S.A.* **112**, E3639 (2015).
 - [32] Y.-K. Yu, P. Taylor, and E. Terentjev, *Phys. Rev. Lett.* **81**, 128 (1998).
 - [33] S. Kumar and S. Mishra, *Phys. Rev. E* **102**, 052609 (2020).
 - [34] S. Kumar and S. Mishra, *Phys. Rev. E* **106**, 044603 (2022).
 - [35] P.-G. De Gennes and J. Prost, *The Physics of Liquid Crystals* (Oxford University Press, 1993).
 - [36] S. Edwards and J. Yeomans, *EPL* **85**, 18008 (2009).
 - [37] A. A. Amsden and F. H. Harlow, *J. Comput. Phys.* **6**, 322 (1970).
 - [38] B. Diény and B. Barbara, *Physical Review B* **41**, 11549 (1990).
 - [39] M. J. Gingras and D. A. Huse, *Physical Review B* **53**, 15193 (1996).
 - [40] L. Giomi, *Phys. Rev. X* **5**, 031003 (2015).